NASA Technical Memorandum 105260

Engine Panel Seals for Hypersonic Engine Applications: High Temperature Leakage Assessments and Flow Modelling

Bruce M. Steinetz
National Aeronautics and Space Administration
Lewis Research Center
Cleveland, Ohio

Rajakkannu Mutharasan and Guang-Wu Du
Drexel University
Philadelphia, Pennsylvania

Jeffrey H. Miller
Sverdrup Technology, Inc.
Lewis Research Center Group
Brook Park, Ohio

and

Frank Ko
Drexel University
Philadelphia, Pennsylvania

Prepared for the
Fourth International Symposium on Transport
Phenomena and Dynamics of Rotating Machinery
sponsored by the Pacific Center of Thermal-Fluids Engineering
Honolulu, Hawaii, April 5-8, 1992

NASA

Trade names or manufacturers' names are used in this report for identification only. This usage does not constitute an official endorsement, either expressed or implied, by the National Aeronautics and Space Administration.

ENGINE PANEL SEALS FOR HYPERSONIC ENGINE APPLICATIONS: HIGH TEMPERATURE LEAKAGE ASSESSMENTS AND FLOW MODELLING

Bruce M. Steinetz
National Aeronautics and Space Administration
Lewis Research Center
Cleveland, OH 44135

Rajakkannu Mutharasan & Guang-Wu Du
Drexel University
Philadelphia, PA 19104

Jeffrey H. Miller
Sverdrup Technology, Inc.
Lewis Research Center Group
Brook Park, OH 44142

Frank Ko
Drexel University
Philadelphia, PA 19104

ABSTRACT

A critical mechanical system in advanced hypersonic engines is the panel-edge seal system that seals gaps between the articulating horizontal engine panels and the adjacent engine splitter walls. Significant advancements in seal technology are required to meet the extreme demands placed on the seals, including the simultaneous requirements of low leakage, conformable, high temperature, high pressure, sliding operation. In this investigation, the seal concept design and development of two new seal classes that show promise of meeting these demands will be presented. These seals include the ceramic wafer seal and the braided ceramic rope seal.

The paper presents key elements of leakage flow models for each of these seal types. Flow models such as these help designers to predict performance-robbing parasitic losses past the seals, and estimate purge coolant flow rates. Comparisons are made between measured and predicted leakage rates over a wide range of engine simulated temperatures and pressures, showing good agreement.

INTRODUCTION

Key to the development of a single stage earth-to-orbit vehicle is an advanced propulsion system that must be integrally designed with the vehicle airframe as conceptually shown in Fig. 1. To maintain sufficiently high specific impulse to reach orbital velocity (Mach 25), hydrogen-burning ramjet/scramjet engines such as shown in Fig. 2 are being developed. To prevent the extremely hot, pressurized engine flow path gases from escaping past the movable panels (see nozzle panel in Fig. 2), high temperature, flexible, sliding seals are required around the panel perimeters. Calculations have shown that at a Mach 6 flight condition engine pressure differentials can reach 100 psi with engine static temperatures higher than 5000°F, ref. 1. These conditions illustrate the severe aero-thermal environment in which the seals must operate.

Complicating the sealing challenge further is the need for the panel-edge seals to seal against severely distorted engine sidewalls. The high heating rates and pressures of hypersonic flight can cause the weight-minimized engine sidewalls to deflect in some cases upwards of 0.15 in. Minimizing leakage past the movable panels requires that the panel-edge seals be sufficiently compliant and preloaded to seal against the engine wall curvature.

To meet the technically challenging design requirements outlined above, NASA Lewis is developing two new classes of engine panel seals as shown in Fig. 3.

Ceramic Wafer Seal: The ceramic wafer seal consists of a stack of ceramic elements mounted in a seal channel along the edge of the movable engine panel. The seal conforms to engine wall distortions by relative sliding of adjacent wafers. Various techniques can be used to transversely preload the ceramic wafers against the engine

wall. In Fig. 3 a series of actively-cooled, pressurized metal bellows forces the wafers to follow the serpentine-distorted engine sidewall. At engine stations where anticipated temperatures exceed the maximum-use temperature of the seal material (2300-2500°F), some form of active cooling such as film or transpiration cooling must be used.

Braided Ceramic Rope Seal: The braided ceramic rope seal (Fig. 3) can be fabricated using either two- or three-dimensional braid architectures. Two-dimensional rope seals were selected for evaluation because of their greater resistance to leakage flow. Braiding the seal from engineered ceramic fibers allow the seals to operate at temperatures over 2000°F. Some form of active preload is required to accommodate the adjacent wall distortions and resist leakage flow during operation. One approach shown in the figure is the cooled pressurized metal bellows.

The primary objectives of this paper are to present the high temperature leakage performances of the wafer and braided rope seals measured using specialized test fixtures; review the development of leakage flow models that enable designers to estimate the flow past the seals; and compare the predicted and measured leakage rates over a broad temperature and pressure range.

EXPERIMENTS

SEAL SPECIMENS

The ceramic wafer specimens tested were 0.5 in. square by 0.13 in. thick. The wafers were made of high purity aluminum oxide having an upper temperature limit of 2500°F. A detailed listing of the ceramic material, thermal and mechanical properties, and relative ranking of competing monolithic ceramics can be found in ref. 2.

The braided rope seal specimens investigated were made either of glass or ceramic fibers depending on intended use temperature. The E-glass fibers were selected at the beginning of these studies for room temperature evaluation because of their relatively low cost and similar sized tows (i.e. 812 denier) when compared to Nextel[1] ceramic fibers. Eight seal specimens were made and designated A1-H1. Their architectural parameters including braid angle, number of longitudinal yarns and number of braiding yarns are summarized in Table I. Measurements made on these seals (ref. 3) established architectural trends showing low leakage. These studies revealed that seals having relatively high percent longitudinal core fibers had lower leakage rates.

Based on these findings, seals K1 and M1 were made with high degree of longitudinal core fibers to assess the high temperature leakage performance. The K1 and M1 seals were fabricated of 900 denier Nextel 312 fiber tows per the architectural specifications in Table I, resulting in 88% and 94% longitudinal core fibers respectively. Nextel fibers were selected because tests have shown that they maintain tensile strength and flexibility at temperatures up to 2300°F.

Wafer Seal Apparatus and Procedures

Leakage measurements for the ceramic wafer seals were performed using the high temperature panel-edge seal rig shown schematically in Fig. 4. A detailed description of the design and development of this test fixture can be found in ref. 4. A brief overview of the test fixture and procedures are repeated herein. Comparable to seal lengths in the engine, three foot seal specimens were tested in the Inconel test fixture shown in Fig. 5. The ceramic wafers were preloaded against the adjacent sidewall using a series of 0.5 in. diameter welded Inconel bellows (located on 1 in. centers) that exerted force on the wafers through a thin Inconel seal backing plate. The bellows were pressurized up to 120 psi which caused an average contact pressure of ≈50 psi (i.e. bellows pressure divided by the ratio of projected seal and bellows areas; see ref. 5)

Procedure: Wafer seal leakage rates were measured at four temperatures ranging from room temperature to 1350°F. Heated air was supplied to the base of the seal as shown in Fig. 4. At each temperature, the engine simulated pressure was varied typically from 100 psi down to 10 psi and then back up to 100 psi for at least one complete pressure cycle. In several cases, the seal leakage rates were measured for multiple pressure cycles to establish seal leakage repeatability. Prior to heating, the wafers were first preset to the preferred sealing

[1]Trade names or manufacturer's names are used in this report for identification only. This usage does not constitute an official endorsement, either expressed or implied by the National Aeronautics and Space Administration.

position (i.e. in contact with the front wall and in contact with the top of the seal channel) using the engine pressure and the lateral preload (≈50 psi seal contact pressure). The wafers were axially compressed with 10 lb (or 40 psi contact pressure for the 0.5 in. square seal) using both left and right axial preloaders (see Fig. 4).

Rope Seal Apparatus and Procedures

Two flow fixtures were used to investigate the braided rope seal leakage performance. For room temperature developmental tests, the one foot room temperature fixture was used, (see Fig. 6). Lateral preloads were applied to the back of the seal with the inflatable rubber diaphragm at either 80 or 130 psig. High temperature leakage measurements were made using the high-temperature panel-edge seal fixture described previously. Lateral preloads up to 80 psi were applied uniformly to the back of the seal using the metal bellows described.

Procedure: For room and high temperature tests, the air pressure was steadily increased and the resulting leakage flow rates were measured for each of the preloads considered. Seal K1 was tested in the as-fabricated condition. Seal M1 was heat treated to the manufacturer's recommendation (12 hrs at 1700 °F), to make the fibers more resistant to physical degradation in steam environments. High temperature performance measurements could not be made for seal M1 because its thin outer sheath incurred damage upon installation and removal from the test rig. Seal K1 was not damaged in this way and was flow tested.

RESULTS & DISCUSSION

CERAMIC WAFER SEAL

The ceramic wafer leakage rates were measured over the anticipated engine pressure loads at engine-simulated air temperatures of 73, 200, 940, and 1350°F, as shown in Fig. 7. The seal leakage rates for each of the temperatures examined were below the industry-established tentative leakage limit of 0.004 lb/s-ft (see ref. 1) shown as the dashed horizontal line for reference purposes in each of the figures. Leakage rates generally decreased with increasing temperature up to moderate temperatures at which point the trend reversed and a slight increase in leakage rates was observed. An explanation for this leakage temperature-dependence is given below where the measured and predicted leakage rates are compared.

Comparison of Measured and Predicted Leakage Rates: The wafer seal leakage flow equation (Eqn. (A7)) presented in Appendix A has been used to predict the leakage as a function of temperature and pressure. The results of these calculations are shown in Figs. 8, 9, and 10 along with the measured results. In each of these curves the measured results are shown with a solid line and the predictions made using the equation are shown with the dashed line. As is well known, gas viscosity increases with temperature. Throughout these analyses the power law of gas viscosity: $\mu = \mu_o(T/T_o)^{2/3}$ (ref. 6) was used for the air viscosity.

In Fig. 8, the measured and predicted leakage rates are compared for a fixed engine pressure differential of 20 psi. The correlation between the predicted and measured leakage rates is very good for the full temperature range. In Fig. 9, the measured and predicted leakage rates are compared for a fixed engine pressure differential of 40 psi. The correlation between the predicted and measured leakage rates is reasonable for this pressure differential. The maximum discrepancy between the measured and predicted rates was slightly over 20 percent and occurred at intermediate temperatures of about 500°F. This discrepancy narrowed to about 14 percent at gas temperatures of 1350°F.

Comparisons are made between the measured and predicted leakage rates at the maximum expected pressure differential of 100 psi in Fig. 10. Examining Fig. 10, it is noted that both the measured trends of decreasing leakage followed by slightly increasing leakage are properly modeled by Eqn. (A7). For this pressure case the maximum discrepancy between the predicted and measured rates was about 38 percent at 500°F. However, at 1350°F the discrepancy between measured and predicted rates was only 18 percent.

Discrepancies as noted above can be caused by several sources. The most probable cause is thermally-induced non-uniform changes in the size and shape of the film-heights (h_f). Since the flow responds to changes in gap height cubed one can see why thermally induced changes in contact condition can lead to appreciable changes in leakage. As an example, analytically changing gap height by 11 percent results in a 38 percent change in leakage. This observation underscores the need to maintain small gaps through optimal loading, wafer design, and tolerances.

It is noted that even though some modeling discrepancies are observed, the absolute magnitude of the leakage rates are still below the industry-established tentative leakage limit, shown by the horizontal dashed line in the figures.

BRAIDED ROPE SEAL

The braided rope seal leakage rates were also assessed over the full range of anticipated pressure loads at several engine simulated temperatures. Leakage rates for seal K1 are shown in Fig. 11 for air temperatures of 80, 450, 930 and 1330 °F for two lateral preloads. As was expected, leakage rates were lower for the higher lateral preload since the preload improves the packing density of the braided structure.

Leakage rates were relatively high at room temperature and steadily decreased as the temperature was increased. At room temperature the seal met the tentative leakage limit (ref. 1) for pressure differentials of about 15 psi. At higher temperatures, the leakage mass flow is considerably less since the gas viscosity is greater and the gas density is lower. At 1330 °F the seal met the tentative leakage flow limit for pressure differentials up to 60 psi.

Comparison of Measured and Predicted Leakage Rates: The braided rope seal leakage flow equation (Eqn. (B4)) developed in Appendix B was used to predict the leakage rates as a function of temperature and pressure. In Fig. 12, the measured and predicted leakage rates are compared for a fixed pressure differential of 10 psi, and a preload of 80 psi. The characteristic dimension used for the predictions throughout the current investigation was $\phi D = 1.40 D_{f,avg}$ as developed in Appendix B. The predicted values are shown for two porosity levels. The minimum porosity ϵ_{min} represents the porosity of a uniform packed bed of elliptical fibers each in intimate contact with their neighbors, as calculated in Appendix B. The second porosity ϵ_{avg} represents the seal porosity determined from the apportionment of the seal's sheath and core porosities, also calculated in Appendix B. Note that by this porosity definition, the seal is treated as a homogeneous fiber bed having a single average porosity (ref. 3, Model I). Excellent agreement is exhibited between the predicted and measured leakage rates in Fig. 12 for the average porosity.

In Fig. 13 the measured and predicted leakage rates are presented for a pressure differential of 35 psi and a preload of 80 psi. Good agreement between the measured and predicted is exhibited over nearly the full temperature range. At room and moderate temperatures the model over-predicted the leakage rate, resulting in a conservative estimate of leakage flow. Work in-progress is investigating the effect of preload and engine pressure on seal flow resistance, which may explain part of the noted discrepancy.

Fiber Diameter Effect: The leakage rates measured for this seal were higher than anticipated from previous room temperature investigations with seals made of E-Glass having similar architectures. The main cause of this difference is attributed to Nextel fibers used to fabricate the seal that were considerably larger than anticipated. The fiber diameter supplied by the manufacturer was claimed to be 10-12 microns. The average Nextel fiber diameter determined using scanning electron micrograph (SEM) techniques was 13.7 microns. Due to the leakage flow dependence on (ϕD) squared, one would expect a seal made to the same architecture as K1 but with the smaller 10 micron filaments would have about half (i.e. $(10/13.7)^2$) the leakage rates as those shown herein. Furthermore, seals made of smaller (8 micron) commercially available Nextel fibers should have even better leakage performance, based on this theoretical trend.

SUMMARY

Two panel-edge seal concepts showing promise of meeting many of the demanding challenges of advanced hypersonic engine environments have been presented. The ceramic wafer seal consists of a stack of high temperature (>2000°F) engineered-ceramic wafers mounted along the edge of the articulating engine panels. The wafers accommodate the anticipated adjacent engine wall distortions by relative sliding between adjacent wafers. The braided ceramic rope seal is made of high temperature ceramic fibers that maintain strength and flexibility at temperatures in excess of 2000°F. These rope seals are also mounted along the panel edges and can be preloaded in several ways, including using the bellows approach discussed.

The high temperature leakage performance of each of these seals was assessed using a specially developed panel-edge seal test fixture at NASA Lewis Research Center. The wafer seal met the tentative leakage flow limit over the full anticipated temperature range for temperatures ranging from room temperature to 1350°F.

The braided rope seal exhibited higher leakage rates than the wafer seal. The rope seal met the tentative leakage limit for an engine pressure differential of 15 psi at room temperature and 60 psi at 1330°F.

The braided rope seal leakage rates were higher than were expected based on previous experience with braided seals because the seal fibers were larger and less uniform than anticipated. Although 10-12 micron fibers were to have been supplied by the manufacturer, the average Nextel fiber diameter measured using SEM techniques was 13.7 microns. Examining the rope seal flow models, the filament diameter plays a large role in seal leakage resistance. Seal leakage resistance is inversely proportional to the filament diameter squared. Hence one would expect that if all other parameters were held constant, a seal made with 10 micron fibers would leak about one-half as much (i.e. $(10/13.7)^2$) as the seal investigated herein, greatly improving the leakage performance of the seal.

Leakage flow models are presented for both of the seals that enable designers to estimate the performance-robbing parasitic leakage past the seals or conversely the coolant flow past the seals, as a function of pressure and temperature. Correlation between the measured and predicted ceramic wafer seal leakage rates is quite good for low to moderate pressure differentials. At the highest anticipated pressure differentials, the model predicts the general decreasing/increasing leakage trends but somewhat under-predicts the observed leakage rates.

The braided rope seal leakage model presented is based on Kozeny-Carmen relations for flow through porous media. The model treats leakage flow through and around the braided seal structure as a system of flow resistances analogous to a series of resistors in an electrical network. These elemental resistances are combined in accordance with the electrical analog to form an overall effective seal resistance that characterizes the seal. Correlation between the measured and predicted values is good for low engine pressures across the wide temperature range examined. At moderate engine pressures the model somewhat overpredicts the room temperature leakage but predicts the high temperature leakage very well.

REFERENCES

1. Steinetz, B.M., DellaCorte, C., and Sirocky, P.J., "On The Development of Hypersonic Engine Seals," NASA TP-2854 (1988).
2. Steinetz, B.M.: "Evaluation and Ranking of Candidate Ceramic Wafer Engine Seal Materials," NASA TM-103795, (1991).
3. Mutharasan, R; Steinetz, B.M.; Tao, X; Ko, F: "Development of Braided Rope Seals for Hypersonic Engine Applications Part II: Flow Modelling," AIAA-91-2495 also NASA TM-104371, (1991).
4. Steinetz, B.M., "A Test Fixture for Measuring High-Temperature Hypersonic Engine Seal Performance," NASA TM-103658 (1990).
5. Steinetz, B.M.: "High Temperature Performance Evaluation of a Hypersonic Engine Ceramic Wafer Seal," NASA TM-103737, (1991).
6. White, F, Fluid Mechanics, McGraw-Hill, New York (1979).
7. Ausman, J.S., "Gas Lubricated Bearings," Advanced Bearing Technology, NASA SP-38, E.E. Bisson and W.J. Anderson, eds., pp. 109-138 (1964).
8. Constantinescu, V.N., Gas Lubrication, American Society of Mechanical Engineers, New York (1969).
9. Scheidegger, A. E., "The Physics of Flow Through Porous Media," revised ed., University of Toronto Press, Toronto, (1960).
10. Bennett, C.O. and Myers, J.E: Momentum, Heat and Mass Transfer, Third edition, McGraw-Hill Book Company, New York, (1982).

TABLE I: BRAIDED ROPE SEAL CONSTRUCTION

Sample No.	Braid Ang. (°)	No. Long. Yarns	No Braid Yarns	Material
A1	45	935	1008	E-Glass
B1	30	935	1248	E-Glass
C1	10	935	1320	E-Glass
D1	45	1497	792	E-Glass
E1	30	1497	840	E-Glass
F1	10	1497	1206	E-Glass
G1	45	2042	312	E-Glass
H1	30	2042	408	E-Glass
K1	45	2302	216	Nextel 312
M1	45	2450	120	Nextel 312

APPENDIX A -- CERAMIC WAFER SEAL LEAKAGE FLOW MODEL

Nomenclature:

$\dot{m}/L$ = *mass flow per unit length*
P = *pressure, abs*
T = *temperature, abs.*
g = *inter-panel gap width*
H_1, H_2 = *seal-to-wall contact dims.*
h_1, h_2 = *seal film heights*
R = *gas constant*
U = *seal velocity* ($\approx$0)
u = *leakage gas velocity*
t = *time*
L = *seal length*
N = *number of wafer interfaces*
F = *force*
M = *moment*
x, y = *coordinate directions*

Greek:
α = *coeff. of thermal expansion*
ρ = *gas density*
μ = *gas viscosity*
μ_o = *room temp. viscosity*

Subscripts:
1, 2 = *seal top and nose surfaces*
s = *supply*
o = *exhaust*
eff = *effective*
CTE = *coeff. of thermal expansion*
v = *variable film height*

A closed form seal leakage flow model has been developed in ref. 5 to predict seal leakage response for the ceramic wafer seal over the wide range of engine pressures and temperatures. The important results of the flow model development are repeated here for reference purposes. During tests three leakage paths were identified for the wafer seal (Fig. 14), including: (1) between the wafer and the top surface of the seal channel accounted for below by the $h_{1,v}$ term; (2) between the seal nose and the adjacent wall accounted for by the $h_{2,v}$ term (where the v denotes variable film height); and (3) at high temperatures through the inter-wafer gaps caused by differential seal and engine panel thermal expansion, accounted for by the h_{CTE} term. Experimental measurements also indicated that the driving potential for each of these leakage paths was the engine supply pressure, P_s. Therefore the seal leakage mass flow rate is the sum of these parallel leakage paths:

$$\dot{m}/L = \dot{m}_1/L + \dot{m}_2/L + \dot{m}_3/L \tag{A1}$$

Expressions for each of these components of the mass flow rate are derived from the basic Reynolds flow equation (ref. 7) where the flow is assumed to be laminar

$$\frac{\partial}{\partial x}\left(\rho h^3 \frac{\partial P}{\partial x}\right) + \frac{\partial}{\partial y}\left(\rho h^3 \frac{\partial P}{\partial y}\right) = 6\mu U \frac{\partial}{\partial x}(\rho h) + 12\mu \frac{\partial(\rho h)}{\partial t} \tag{A2}$$

Considerable simplifications can be made to this equation, since: (1) the seal is long relative to the effective gaps; (2) the seal moves slowly across the wall ($U \approx 0$); and, (3) only the steady-state solution is desired. The remaining lead term is further simplified using the ideal gas law (refs. 7-8) to result in the following equation that is solved for the pressure distribution within the thin gaps:

$$\frac{\partial}{\partial x}\left(Ph^3 \frac{\partial P}{\partial x}\right) = 0 \tag{A3}$$

Solving this equation using the uniform flow area assumption results in equations for pressure as a function of distance through the gaps.

The unit mass flow through the small gap separating the seal and the adjacent wall is found by integrating the velocity profile over the film height h:

$$\dot{m}/L = \int_0^h \rho u dy \tag{A4}$$

Assuming a laminar velocity profile with the no-slip boundary conditions; integrating over the area; using the ideal gas law relation; and solving for the requisite pressure distribution from Eqn. (A3), results in the following expression for the regions denoted 1 & 2 between the wafer and the adjacent surfaces:

$$\dot{m}/L = \frac{(P_s^2 - P_o^2)}{24\mu RT}\left(\frac{h_1^3}{H_1} + \frac{h_2^3}{H_2}\right) \tag{A5}$$

Leakage Pressure-Dependence: According to the flow Eqn. (A5) the leakage flow rate varies with the difference in the squares of the pressure, (see short dashes in Fig. 15). Good correlation between the measured and predicted leakage rates was observed for pressure differentials less than 50 psi. However the leakage model over predicts the measured leakage rates by 53 percent, at pressure differentials of 100 psi. The likely cause of the discrepancy is the film heights h_i are not constant but are actually reduced in size as the pressure differential applied across the seal is increased. Fig. 14 depicts the forces leading to smaller film thickness as the pressure differential is increased.

Using Eqn. (A5) effective film heights were back-calculated as a function of pressure drop across the seal. The film height decreases nearly linearly with increasing pressure differential (ref. 5). A least squares regression analysis performed resulted in a strong (correlation coefficient of $R^2 = 0.98$) correlation for a straight line fit through the data points. The resulting linear equation is:

$$h_{1,v} = h_{2,v} = 4.95x10^{-5} - 1.131x10^{-7}(P_s - P_o) \qquad \text{(A6)}$$

$$h_{i,v} = ft; \quad P_s, P_o = lb/sq\text{-}in.$$

Implementing this variable film thickness into Eqn. (A5) one can recalculate mass flow versus pressure drop. The agreement between measured and predicted leakage rates is very good (see long dashes in Fig. 15). The maximum observed discrepancy at room temperature is only 6 percent.

Thermal Expansion Differences: The coefficient of thermal expansion (CTE) of the aluminum-oxide wafers used in these investigations is nominally half the CTE of the test rig (representing the engine panel) made of engine simulated material (i.e., Inconel). As the three foot rig heats up it axially expands more than the ceramic wafers. The inter-wafer gap is of the same order of magnitude as the film-heights calculated between the seal and the adjacent wall surfaces, and must be accounted for in the model. Flow between wafers represents the third parallel leakage path which can be added to the basic leakage flow Eqn. (A5) resulting in:

$$\dot{m}/L = \frac{(P_s^2 - P_o^2)}{24\mu RT}\left(\frac{h^3_{1,v}}{H_1} + \frac{h^3_{2,v}}{H_2} + \frac{Ngh^3_{CTE}}{LH_2}\right) \qquad \text{(A7)}$$

$$h_{CTE} = (\alpha_{engine\ panel} - \alpha_{wafers})\frac{L\Delta T}{N}$$

APPENDIX B - BRAIDED ROPE SEAL LEAKAGE FLOW MODEL DEVELOPMENT

Nomenclature

A_c = *Cross sect. flow area*
= *gap x seal length*
A_y = *Yarn cross sect. area*
D_f = *Fiber diameter*
g = *Inter-panel gap width*
g_c = *Gravity constant*
$\dot{m}$ = *Mass flow rate of gas*
M_w = *Gas molecular weight*
N_c = *Number of core yarns*
N_s = *Number of sheath yarns*
P_o = *Pressure downstream of seal*
P_s = *Pressure upstream of seal*
R_g = *Universal gas constant*
T = *Absolute temperature*
t,t_1, = *Seal dimensions; Fig 16*
u = *Superficial gas velocity*
$2y_o$ = *Seal/housing clearance*
Re = *Reynolds No.* = $\frac{\phi D_{f,avg}\rho u}{\mu(1-\epsilon)}$

Greek:

ϵ = *Porosity*
ϕ = *Shape factor*
θ = *Braid ang.*
ρ_f = *Fiber density*
μ = *Gas viscosity*
ρ = *Gas density*
λ = *Fiber ellipticity ratio*
= $\frac{Semi\text{-}major\ \ dia.}{Semi\text{-}minor\ \ dia.}$

Subscripts:

a = *Semi-major*
b = *Semi-minor*
c = *Core*
e = *Edge*
sl = *Seal*
s = *Sheath*
avg = *Average*
min = *Minimum*
1..3 = *Flow paths; Fig 16*

The leakage flow model for the braided rope seal was developed by the authors in ref. 3 and was derived from the Kozeny-Carmen equations for flow through porous media. New insight gained by the current investigation has led to several refinements to the original model in the areas of fiber cross section, fiber shape factor, and the treatment of seal porosity. These refinements plus the basis of the flow model are outlined herein.

The model allows estimates of gas leakage as a function of fiber diameter, rope seal porosity, gas properties, and pressure drop across the seal for seals flowing in the laminar regime, Re < 10. As shown in Fig. 16, the flow across the rope seal can be divided into two categories: (1) flow through the seal and (2) flow around seal.

1. Flow through seal

The Kozeny-Carmen equation (ref. 9) provides an expression relating the gas velocity through the porous media to the pressure drop across the seal:

$$u = \frac{-(P_o - P_s)g_c}{150\dfrac{\mu t}{(\phi D)^2}\dfrac{(1-\epsilon)^2}{\epsilon^3}} \tag{B1}$$

An expression for the mass flow rate through the seal is found by integrating this expression over the area, where ideal gas behavior is assumed and the gas density is evaluated at the average value based on the two end-points:

$$\frac{\dot{m}}{L} = \frac{-(P_o^2 - P_s^2)}{300\dfrac{\mu R_g T}{M_w g_c}\dfrac{tL}{A_c}\dfrac{(1-\epsilon)^2}{\epsilon^3(\phi D)^2}} \tag{B2}$$

2. Flow around seal

Edge flow can be treated as flow between parallel non-porous surfaces separated by a small gap. Assuming that the gap between the surfaces can be considered constant and equal to $2y_o$, one can relate the leakage flow rate to the pressure difference across the seal, (ref. 10):

$$\frac{\dot{m}}{L} = \frac{-(P_o^2 - P_s^2)}{\dfrac{3\mu R_g T}{M_w g_c}\dfrac{t}{y_o^3}} \tag{B3}$$

FLOW RESISTANCE

To account for leakage flow through and around the seal, the model treats the two-dimensional braided seal structures as a system of flow resistances analogous to a series of resistors in an electrical network. For the purposes of this model development, resistance is defined as the ratio of the difference in the squares of the upstream and downstream pressure (i.e. the flow potential) to the mass flow per unit seal length (i.e. the current). These resistances are combined as in an electrical network to form an effective seal resistance, R_{eff}:

$$\frac{\dot{m}}{L} = \frac{P_s^2 - P_o^2}{R_{eff}} \quad where \quad \frac{1}{R_{eff}} = \frac{1}{R_1} + \frac{1}{R_2} + \frac{1}{R_3} \tag{B4}$$

where:

$$R_1 = 9K\frac{t}{y_o^3}; \quad R_3 = 3K\frac{t}{y_o^3}; \quad R_2 = 300K\frac{tL}{A_c}\frac{(1-e_{avg})^2}{e_{avg}^3(\phi D_{f,avg})^2}; \; and \; K = \frac{\mu R_g T}{M_w g_c}$$

$$\phi = \frac{area\ of\ sphere\ with\ equivalent\ fiber\ volume}{actual\ surface\ area\ of\ fiber} \tag{B5}$$

$$\phi D = \frac{3\lambda}{\lambda+1}\frac{D_{f,avg}}{0.75\lambda - 0.5\sqrt{\lambda} + 0.75}; \quad D_{f,avg} = \frac{D_{f,a} + D_{f,b}}{2}$$

Calculation Basis

An important parameter in determining flow resistance through the seal is the dimension, D. Considering that the bulk of the seal is made up of longitudinal fibers and that the number of fiber-fiber interfaces is significantly larger than the number of yarn-yarn interfaces, the dimension D was taken as the average fiber diameter, $D_{f,avg}$. Scanning electron photo-micrographs taken of the Nextel fibers revealed elliptical fibers having semi-major and semi-minor diameters. The average fiber diameter found was 13.7 micron and was found by averaging the semi-major and semi-minor diameters of a minimum of 20 fibers. The fiber ellipticity ratio λ of 1.6 was also determined from these measurements. The ellipticity ratio and average fiber diameter were substituted into Eqn. (B5) to compute the characteristic dimension, $(\phi D)=1.40D_{f,avg}$, used for the flow analysis.

Another characteristic dimension is the distance, y_o in calculating seal edge leakage. In the present calculation, the clearance was assumed to be proportional to fiber diameter. Specifically y_o is assumed to be $0.1\,(\phi D)$.

Porosity Determination: To calculate the lower and upper bounds on the seal leakage two porosities were used. The lower leakage bound was calculated using $e_{min} = 1-\pi/4$. This expression gives the minimum porosity for a uniform stack of elliptical cross-sectional fibers in intimate contact with four neighbors. The second seal porosity was determined from Eqn. (B6) which represents the geometry of the fibers and yarns used in producing each of the seal's core and sheath, apportioned to the seal's core and sheath cross sectional areas.

$$e_{avg} = 1 - \frac{A_y N_c + A_y N_s \cos\theta}{t^2} \qquad \text{(B6)}$$

Figure 1.—Hypersonic vehicle powered by ramjet/scramjet engines.

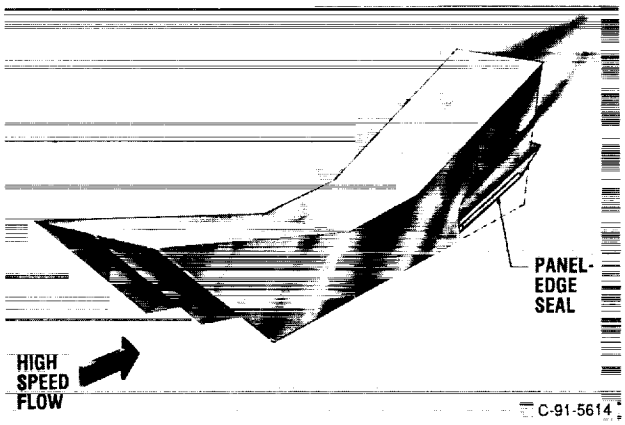

Figure 2.—Schematic of hypersonic engine showing the integrated articulating engine panels and panel-edge seal.

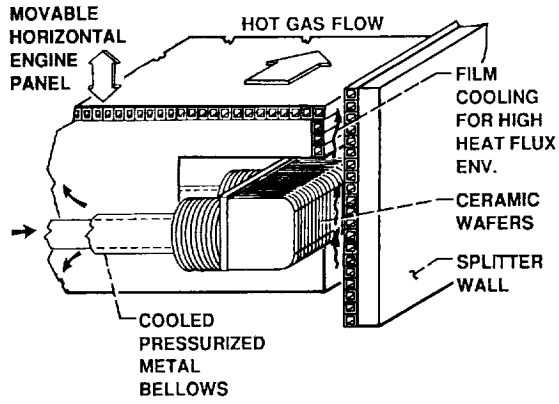

(a) Ceramic wafer seal.

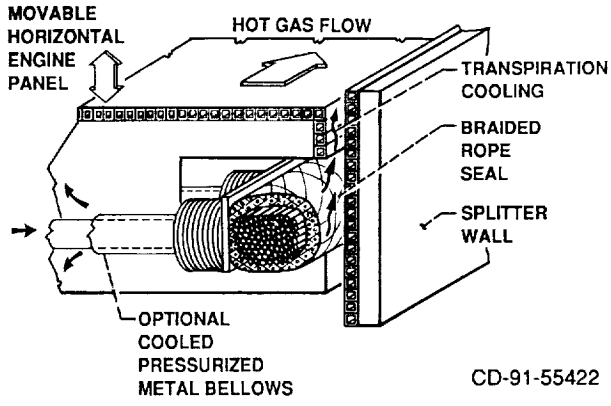

(b) Braided ceramic rope seal.

Figure 3.—Isometric of engine panel seals under development: (a) ceramic wafer seal; (b) braided ceramic rope seal.

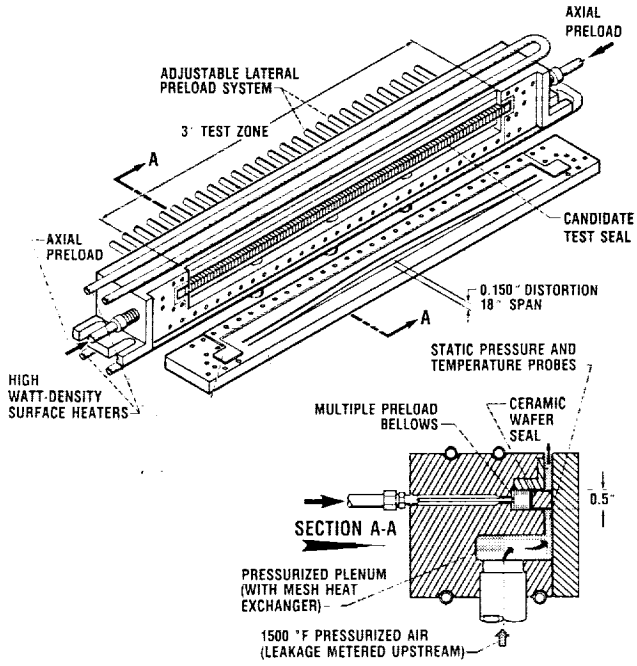

Figure 4.—Schematic of high temperature panel-edge seal test fixture.

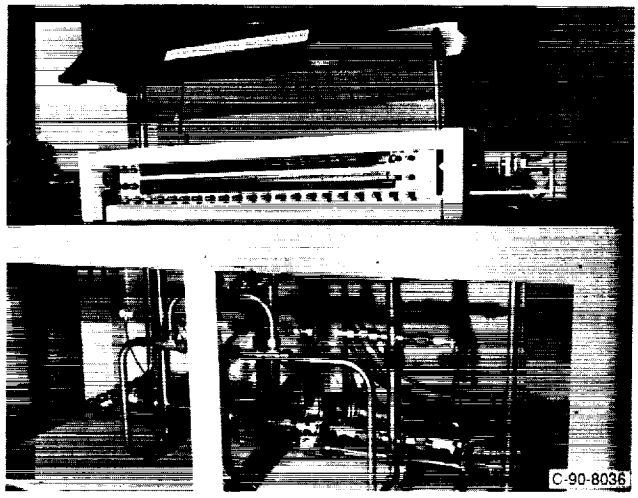

Figure 5.—Photo of high temperature seal test rig, front wall removed for clarity.

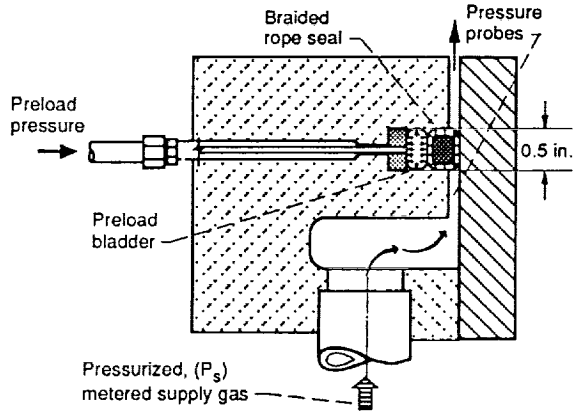

Figure 6.—Cross-section of room temperature braided rope seal leakage test fixture.

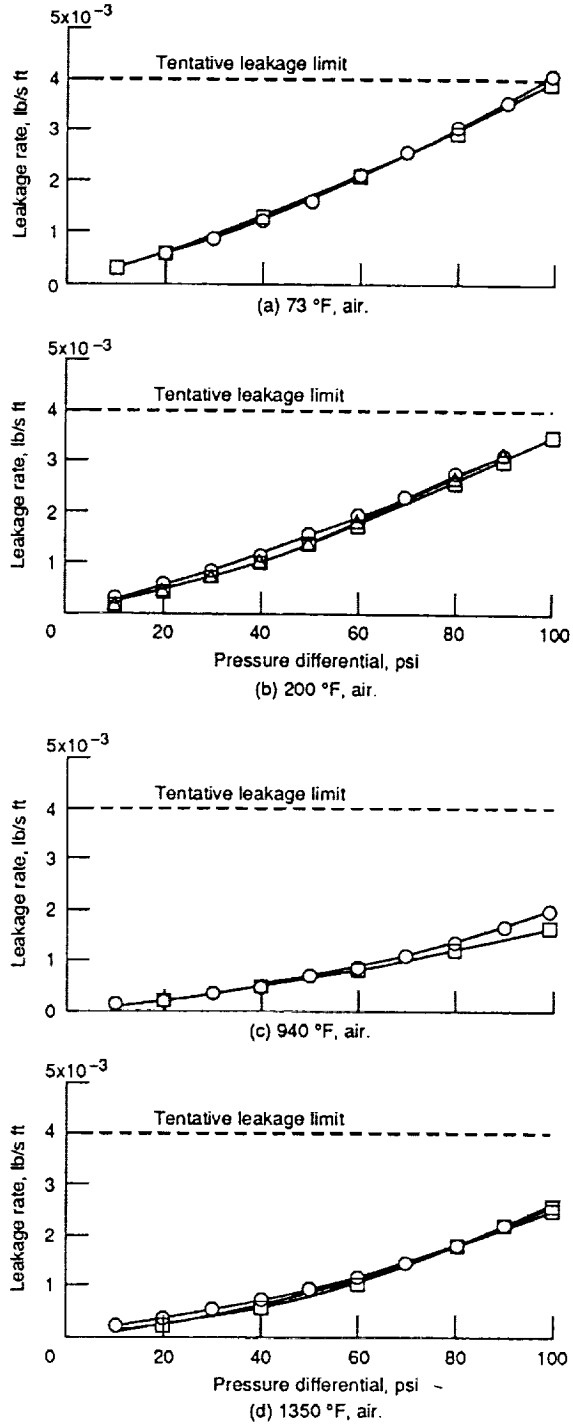

Figure 7.—Ceramic wafer seal measured seal leakage rates versus simulated engine pressure differential.

ORIGINAL PAGE
BLACK AND WHITE PHOTOGRAPH

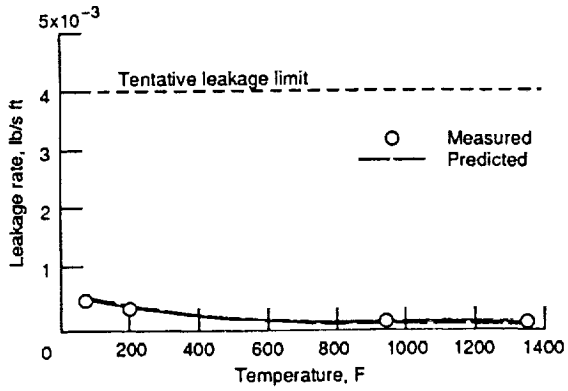

Figure 8.—Comparison of measured and predicted ceramic wafer seal leakage rates as a function of temperature for a fixed engine pressure differential of 20 psi.

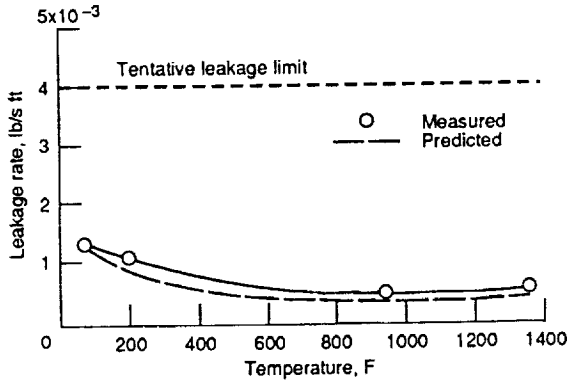

Figure 9.—Comparison of measured and predicted ceramic wafer seal leakage rates as a function of temperature for a fixed engine pressure differential of 40 psi.

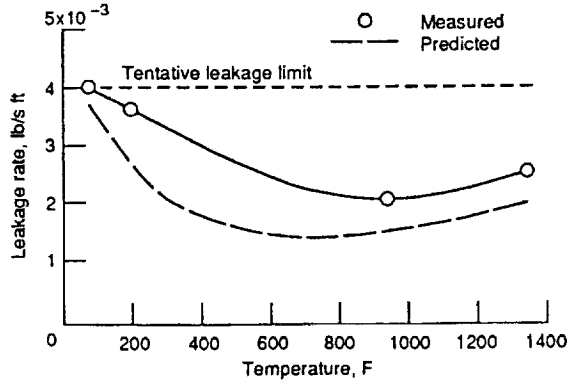

Figure 10.—Comparison of measured and predicted ceramic wafer seal leakage rates as a function of temperature for a fixed engine pressure differential of 100 psi.

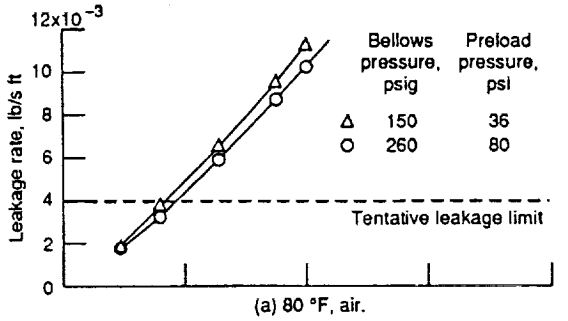

(a) 80 °F, air.

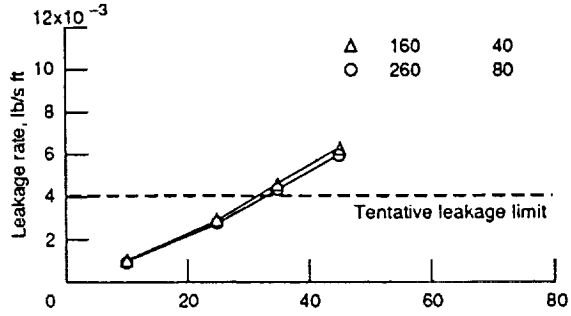

(b) 450 °F, air.

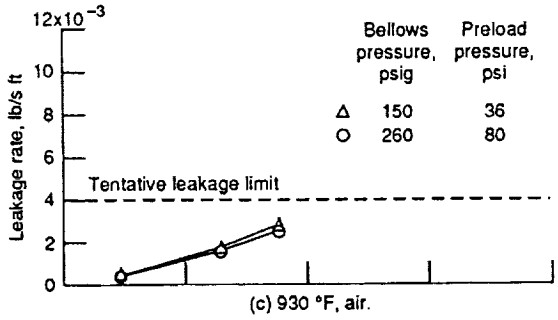

(c) 930 °F, air.

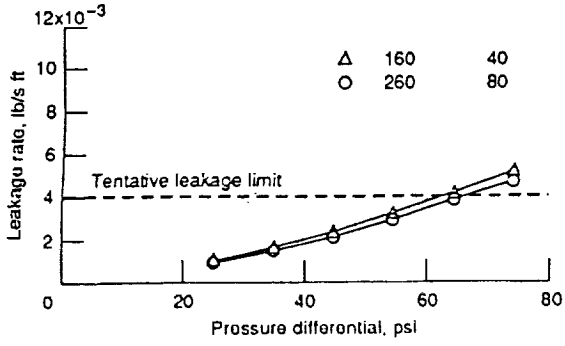

(d) 1330 °F, air.

Figure 11.—Braided ceramic rope seal (K1) leakage rates versus simulated engine pressure differential.

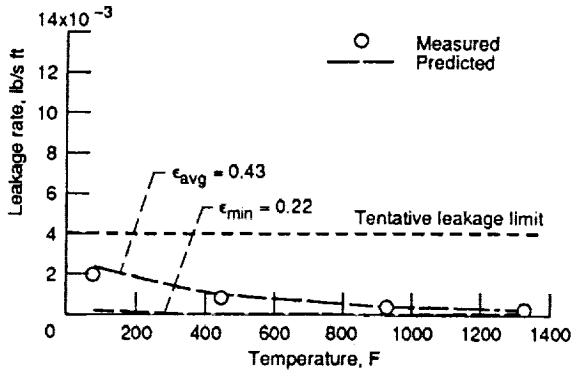

Figure 12.—Comparison of measured and predicted braided rope seal (K1) leakage rates as a function of temperature for a fixed engine pressure differential of 10 psi.

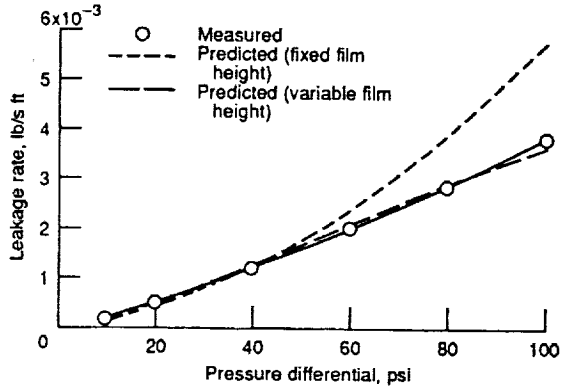

Figure 15.—Comparison of measured and predicted ceramic wafer seal leakage rates versus simulated engine pressure differential using fixed film height and variable film height assumptions.

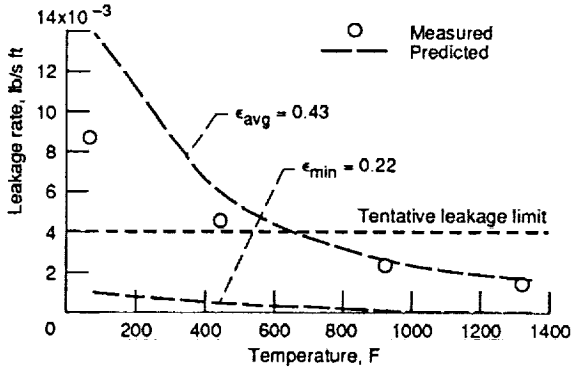

Figure 13.—Comparison of measured and predicted braided rope seal (K1) leakage rates as a function of temperature for a fixed engine pressure differential of 35 psi.

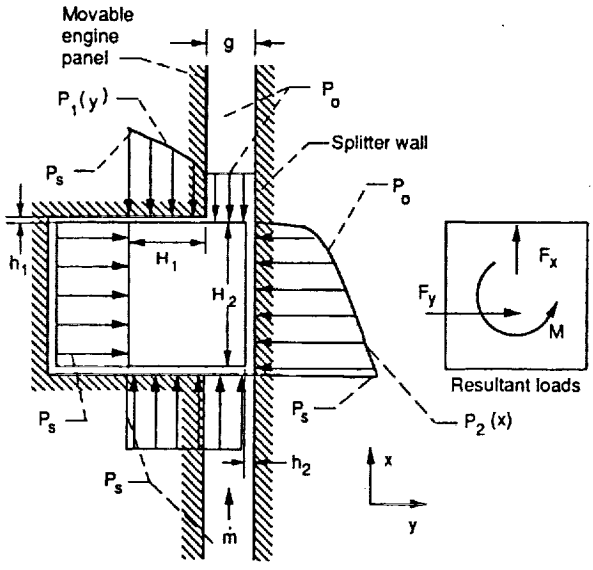

Figure 14.—Ceramic wafer seal flow model variables and pressure balance.

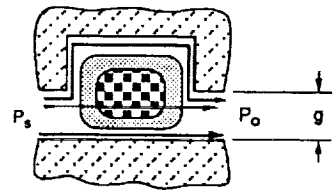

Flow Path	Flow Resistance
1	$R_1 = 9K \frac{t}{y_0^3}$
2	$R_2 = 300K \frac{tL}{A_C} \frac{(1-\epsilon_{avg})^2}{\epsilon_{avg}^3 (\phi D_{f,avg})^2}$
3	$R_3 = 3K \frac{t}{y_0^3}$

Figure 16.—Various flow paths used in calculating total flow resistance for the braided rope seal. The top and bottom paths given above show the flow around the seal. Flow through the seal is modeled by the single homogeneous resistance based on ϵ_{avg}.

REPORT DOCUMENTATION PAGE

Form Approved
OMB No. 0704-0188

1. AGENCY USE ONLY (*Leave blank*)	2. REPORT DATE	3. REPORT TYPE AND DATES COVERED
		Technical Memorandum

4. TITLE AND SUBTITLE

Engine Panel Seals for Hypersonic Engine Applications: High Temperature Leakage Assessments and Flow Modelling

5. FUNDING NUMBERS

WU-505-63-5B

6. AUTHOR(S)

Bruce M. Steinetz, Rajakkannu Mutharasan, Guang-Wu Du, Jeffrey H. Miller, and Frank Ko

7. PERFORMING ORGANIZATION NAME(S) AND ADDRESS(ES)

National Aeronautics and Space Administration
Lewis Research Center
Cleveland, Ohio 44135-3191

8. PERFORMING ORGANIZATION REPORT NUMBER

E-6545

9. SPONSORING/MONITORING AGENCY NAMES(S) AND ADDRESS(ES)

National Aeronautics and Space Administration
Washington, D.C. 20546-0001

10. SPONSORING/MONITORING AGENCY REPORT NUMBER

NASA TM-105260

11. SUPPLEMENTARY NOTES

Prepared for the Fourth International Symposium on Transport Phenomena and Dynamics of Rotating Machinery sponsored by the Pacific Center of Thermal-Fluids Engineering, Honolulu, Hawaii, April 5-8, 1992. Bruce M. Steinetz, NASA Lewis Research Center. Rajakkannu Mutharasan, Guang-Wu Du, and Frank Ko, Drexel University, Philadelphia, Pennsylvania 19104. Jeffrey H. Miller, Sverdrup Technology, Inc., Lewis Research Center Group, 2001 Aerospace Parkway, Brook Park, Ohio 44142 (work funded by NASA Contract NAS3-25266). Responsible person, Bruce M. Steinetz, (216) 433-3302.

12a. DISTRIBUTION/AVAILABILITY STATEMENT

Unclassified - Unlimited
Subject Category 37

12b. DISTRIBUTION CODE

13. ABSTRACT (*Maximum 200 words*)

A critical mechanical system in advanced hypersonic engines is the panel-edge seal system that seals gaps between the articulating horizontal engine panels and the adjacent engine splitter walls. Significant advancements in seal technology are required to meet the extreme demands placed on the seals, including the simultaneous requirements of low leakage, conformable, high temperature, high pressure, sliding operation. In this investigation, the seal concept design and development of two new seal classes that show promise of meeting these demands will be presented. These seals include the ceramic wafer seal and the braided ceramic rope seal. The paper presents key elements of leakage flow models for each of these seal types. Flow models such as these help designers to predict performance-robbing parasitic losses past the seals, and estimate purge coolant flow rates. Comparisons are made between measured and predicted leakage rates over a wide range of engine simulated temperatures and pressures, showing good agreement.

14. SUBJECT TERMS

Glands (seals); Packings (seals); Seals (stoppers); Design; Porous materials; Fluid flow; Ramjet engines

15. NUMBER OF PAGES

14

16. PRICE CODE

A03

17. SECURITY CLASSIFICATION OF REPORT	18. SECURITY CLASSIFICATION OF THIS PAGE	19. SECURITY CLASSIFICATION OF ABSTRACT	20. LIMITATION OF ABSTRACT
Unclassified	Unclassified	Unclassified	